Structural Insights into Calmodulin-regulated L-selectin Ectodomain Shedding*⒮

Jessica L. Gifford[1]**, Hiroaki Ishida, and Hans J. Vogel**[2]

From the Biochemistry Research Group, Department of Biological Sciences, University of Calgary, Calgary, Alberta T2N 1N4, Canada

Background: Calmodulin inhibits the proteolysis of L-selectin's extracellular domains through an unknown mechanism.
Results: Calmodulin binds the juxtamembrane and predicted membrane-spanning regions of L-selectin in a calcium-dependent manner.
Conclusion: Binding of calmodulin to the cytoplasmic/transmembrane domain of L-selectin enacts a conformational change in the extracellular domains preventing cleavage.
Significance: Elucidating the mechanisms of L-selectin shedding is critical to understanding leukocyte trafficking.

The L-selectin glycoprotein receptor mediates the initial steps of leukocyte migration into secondary lymphoid organs and sites of inflammation. Following cell activation through the engagement of G-protein-coupled receptors or immunoreceptors, the extracellular domains of L-selectin are rapidly shed, a process negatively controlled via the binding of the ubiquitous eukaryotic calcium-binding protein calmodulin to the cytoplasmic tail of L-selectin. Here we present the solution structure of calcium-calmodulin bound to a peptide encompassing the cytoplasmic tail and part of the transmembrane domain of L-selectin. The structure and accompanying biophysical study highlight the importance of both calcium and the transmembrane segment of L-selectin in the interaction between these two proteins, suggesting that by binding this region, calmodulin regulates in an "inside-out" fashion the ectodomain shedding of the receptor. Our structure provides the first molecular insight into the emerging new role for calmodulin as a transmembrane signaling partner.

Cell adhesion molecules expressed on leukocytes and endothelial cells intricately coordinate both the transit of granulocytes and monocytes from the bloodstream to inflamed tissue and the homing of naive lymphocytes to peripheral lymphoid organs (1, 2). Described by the adhesion cascade, several adhesion molecule families act to sequentially recruit and tether leukocytes to the vessel wall and then provide firm adhesion to

and subsequent migration through the endothelial cell layer. The selectins are a three-member family of adhesion molecules expressed by leukocytes (L-selectin), platelets (P-selectin), and endothelial cells (E- and P-selectin), which in collaboration with their carbohydrate-presenting ligands execute leukocyte tethering and rolling along the luminal surface of venules that surround peripheral lymphoid organs and sites of inflammation (3).

The three selectins share analogous extracellular domains, including an N-terminal carbohydrate-binding lectin domain known to facilitate the observed rolling behavior of leukocytes despite the hydrodynamic shear force of the bloodstream (Fig. 1A). In contrast, the intracellular tails of these proteins are not conserved, a fact that suggests different modes of regulation and intracellular binding partners for each of the selectins. Although only 17 amino acids long, the cytoplasmic tail of L-selectin has been implicated in concentrating the protein to the tips of microvilli through its interaction with membrane-cytoskeleton cross-linking proteins α-actinin and the ezrin/radixin/moesin (ERM)[3] family (4). The tail is phosphorylated by protein kinase C isozymes as well as Src-tyrosine kinase p56^{lck} (5, 6) and has a key role in the down-regulation of L-selectin by mediating ectodomain shedding (7).

Upon leukocyte activation through the engagement of G-protein-coupled receptors (GPCRs) *in vivo* by cytokines and *in vitro* by phorbol esters, the extracellular domains of L-selectin are rapidly cleaved at a membrane-proximal cut site by tumor necrosis factor α-converting enzyme (TACE) (also known as A disintegrin and metalloprotease-17 (ADAM-17)) (8). This regulatory mode is unique in the selectin family to L-selectin. Once cleaved, the extracellular domains remain attached to their ligands or circulate as a soluble fraction in the plasma, whereas the cytoplasmic and transmembrane domains

---

[3] The abbreviations used are: ERM, ezrin/radixin/moesin; CaM, calmodulin; CSP, chemical shift perturbation; GPCR, G-protein-coupled receptor; HSQC, heteronuclear single quantum coherence; ITC, isothermal titration calorimetry; RDC, residual dipolar coupling; RMSD, root mean square deviation; TACE, tumor necrosis factor α-converting enzyme; BisTris, 2-[bis(2-hydroxyethyl)amino]-2-(hydroxymethyl)propane-1,3-diol; MARCKS, myristoylated alanine-rich C kinase substrate.

Calmodulin-regulated L-selectin Shedding

and 11 amino acid residues of the extracellular portion remain attached to the cell. A key player in the shedding response to leukocyte activation is the ubiquitous calcium (Ca^{2+})-binding protein calmodulin (CaM). Known to regulate numerous effectors involved in growth, proliferation, and movement (9, 10), CaM appears to associate constitutively with the L-selectin tail in resting leukocytes and thereby protects the extracellular domains from proteolytic cleavage (11, 12). Artificial activation of leukocytes with phorbol 12-myristate 13-acetate induces the release of CaM from L-selectin and the shedding of the extracellular domains. It has been proposed that CaM exerts its effects by inducing a conformational change in the extracellular domains that renders the cleavage site resistant to proteolysis, a hypothesis supported by the relaxed sequence specificity but length prerequisite displayed by the cleavage site (13, 14).

To further understand the function of CaM in regulating L-selectin ectodomain shedding, we have examined the interaction between these two proteins at the structural level, in turn studying the requirement for Ca^{2+} as well as the role of the transmembrane domain and juxtamembrane region. We have found that both Ca^{2+} and a limited region of the L-selectin cytoplasmic domain, including a portion of the predicted membrane-spanning region and critical hydrophobic residues therein, are required for tight binding between CaM and L-selectin. A solution-based NMR structure explains the molecular details of this interaction.

EXPERIMENTAL PROCEDURES

Sample Preparation—Unlabeled and isotopically enriched CaM was recombinantly expressed in *Escherichia coli* BL21(DE3) cells containing the pET30b(+) expression vector as described previously (15). For isotope labeling, minimal medium containing ^{15}N and either $^{1}H,^{12}C$- or $^{1}H,^{13}C$-labeled glucose in H_2O or $[^{2}H,^{12}C]$glucose in 99.9% $^{2}H_2O$ was used. To create ($^{1}H/^{13}C$-*methyl*-Met)/$^{2}H/^{15}N$-labeled CaM, 100 mg/liter ^{1}H-α,ϵ-^{13}C-ϵ-^{2}H-labeled methionine was added to the culture 1 h prior to induction with isopropyl β-D-1-thiogalacto-pyranoside (15). CaM samples were purified to homogeneity by Ca^{2+}-dependent phenyl-Sepharose chromatography. All peptides were commercially synthesized (GeneScript) and determined to be more than 95% pure by matrix-assisted laser desportion/ionization mass spectroscopy and high pressure liquid chromatography. The concentration of CaM was determined using the equation, $\epsilon_{276\ nm} = 2900\ M^{-1}\ cm^{-1}$.

Isothermal Titration Calorimetry—All ITC experiments were performed on a MicroCal VP-ITC microcalorimeter. CaM and peptide samples were dissolved in 20 mM HEPES (pH 7.3), 100 or 300 mM KCl, and either 1 mM $CaCl_2$ or 3 mM EGTA and contained 262–889 μM peptide or 20 μM CaM. Data were fitted using the "two sets of sites" model in the MicroCal Origin software to determine the apparent stoichiometry (N), association constant (K_a), and the enthalpy change (ΔH) associated with binding. The ΔH and K_a values were then used to calculate the entropy of binding ($T\Delta S$) through the relationships $\Delta G = -RT\ln K_a$ and $\Delta G = \Delta H - T\Delta S$. The fitted K_a values were converted to K_d values using the relationship $K_d = 1/K_a$. The reported values represent the average and S.D. of three independent titrations performed at 30 °C.

NMR Spectroscopy—NMR experiments were performed on a Bruker Avance 500-MHz NMR spectrometer equipped with a triple resonance, inverse cryogenic probe with a single axis z gradient. Resonance assignments of the backbone and side chain atoms for CaM in complex with LSEL*l* (L-selectin long peptide) were obtained using through-bond heteronuclear scalar couplings with the standard pulse sequences (15). For assignment of the side chain methyl group of the methionines, three-dimensional HMBC and LRCH experiments that record the long range correlations between the Hϵ/Cϵ and Hγ/Cγ atoms were used (16). Resonance assignments as well as intra-peptide NOEs for LSEL*15* (L-selectin 15-mer peptide) in complex with $^{2}H/^{15}N$-labeled CaM were obtained using two-dimensional COSY and two-dimensional F2-isotope-filtered NOESY spectra. Intermolecular NOEs for the ($^{1}H/^{13}C$-*methyl*-Met)/$^{2}H/^{15}N$-labeled CaM·LSEL*15* complex were obtained from three-dimensional ^{13}C-edited NOESY-HSQC spectra. A mixing time of 100 ms was employed for all NOESY spectra. $^{1}D_{NH}$ RDCs were measured using an IPAP-HSQC (17). NMR samples contained 0.2–0.8 mM ^{15}N-, $^{13}C/^{15}N$-, $^{2}H/^{15}N$-, or ($^{1}H/^{13}C$-*methyl*-Met)/$^{2}H/^{15}N$-labeled CaM in 20 mM BisTris (pH 6.8), 100 mM KCl, 0.03% NaN_3, 0.5 mM 2,2-dimethyl-2-silapentane-5-sulfonate, 90% H_2O plus 10% $^{2}H_2O$ or 99.9% $^{2}H_2O$, and either 4 mM $CaCl_2$ or 5 mM EGTA. Samples for RDC measurements contained an extra 200 mM KCl and 16 mg/ml filamentous phage PF1 (Asla Biotech Ltd.) to achieve partial alignment. The increased KCl concentration is required to prevent CaM-phage interactions (15, 18) and did not have an effect on the binding affinity of LSEL*l* for Ca^{2+}-CaM (supplemental Table S1). To avoid the peak broadening that characterizes NMR spectra of the 1:2 interaction, samples of the 1:1 complex between labeled CaM and unlabeled LSEL*l* or LSEL*15* were created through careful titration monitored through ^{15}N or ^{13}C HSQC spectra: 0.1 molar increments of peptide were added to CaM until the cross-peaks of free Ca^{2+}-CaM were replaced with those of the 1:1 spectra. For resonance assignment of the bound peptide, a 0.7:1 molar ratio of peptide to CaM was employed to ensure peptide saturation. ^{1}H, ^{13}C, and ^{15}N chemical shifts in all spectra were referenced using 2,2-dimethyl-2-silapentane 5-sulfonate. Spectra were processed with the NMRPipe package (19) and analyzed using NMRView (20). Chemical shift perturbations (CSPs) in the ^{15}N HSQC spectra of Ca^{2+}-bound and apo-CaM complexed in turn with either the LSEL*l* or LSEL*s* (L-selectin short peptide) peptides were calculated as the weighted average chemical shift difference of the ^{1}H and ^{15}N resonances according to Equation 1 (21).

$$CSP = \sqrt{(\Delta H_N)^2 + (\Delta N/5)^2} \qquad \text{(Eq. 1)}$$

Structure Calculation—To determine the structure of the 1:1 Ca^{2+}-CaM·LSEL*15* complex, a protocol analogous to that published by Gifford *et al.* (15) was employed. Briefly, the PALES software was used to determine the domain orientation of CaM in the complex by fitting 109 measured H_N-N RDCs to those back-calculated from CaM-peptide crystal structures deposited in the Protein Data Bank (22). Following the procedure outlined by Ikura and co-workers (18), only RDCs from structured regions of CaM (as defined by backbone chemical shifts)

were chosen for analysis: residues 6–72 from the N-terminal domain and 85–144 from the C-terminal domain (18, 23). The structure of bound LSEL*15* was solved using CYANA (version 2.0) (24) and subsequently used to derive upper distance limit restraints as well as hydrogen bonding and backbone dihedral angle restraints. CaM-specific information included H_N-N RDCs, hydrogen bond restraints based on chemical shift index-derived secondary structure prediction, backbone dihedral angle restraints both obtained from the RDC-selected starting model and calculated from chemical shifts using TALOS (25), and Ca^{2+} ligand restraints. Distances between CaM and LSEL*15* were provided by intermolecular NOEs between the methionine methyl groups of CaM and amino acid side chains of the bound peptide. Due to the lack of a suitable internal standard through which to calibrate these spectra, peak overlap, and the non-linear intensity of potential methyl-methyl NOEs, the intermolecular NOE distance restraints were binned into one distance class of 1.8–6.0 Å.

The structure calculation of the Ca^{2+}-CaM·LSEL*15* complex was performed using a previously established two-step, low temperature torsion angle simulated annealing protocol in the program Xplor-NIH (version 2.24) (15, 26, 27). Briefly, in the first step, the starting model built from the homologous crystal structure underwent Powell energy minimization and torsion angle dynamics at 200 K followed by simulated annealing in which the temperature was decreased from 200 to 20 K in $\Delta T =$ 10 K steps. The lowest energy structure was selected as the starting model for step 2. In the second step, the structure from step 1 underwent torsion angle dynamics at 20 K followed by simulated annealing in which the temperature was decreased from 20 to 1 K in $\Delta T = 1$ K steps. 100 structures were generated in step 2, and the lowest energy structure was selected for further analysis. The structures were validated by the program PROCHECK (28). Molecular graphics were created using the program MOLMOL (29) or PyMOL (version 1.3).

Molecular Modeling of the CaM·L-selectin·ERM Complex—A model of this heterotrimer was built by overlapping L-selectin residues Arg[356]–Lys[363] shared between the CaM·LSEL*15* complex structure presented here and a pre-existing model of the L-selectin cytoplasmic tail bound to the N-terminal domain of moesin (also known as the FERM (band <u>f</u>our-point one, <u>e</u>zrin, <u>r</u>adixin, <u>m</u>oesin homology) domain) and the C-terminal lobe of CaM (30). The overlay produced an ~1-Å backbone root mean square deviation (RMSD) between the shared residues (supplemental Fig. S1). The resulting heterotrimeric complex was energy-minimized for steric clashes using discrete molecular dynamics in the program Chiron (31).

RESULTS

Identification of the L-selectin CaM Binding Site and Ca^{2+} Specificity of the Interaction—To characterize the interaction between L-selectin and CaM at the molecular level, the roles of Ca^{2+} as well as the juxta- and transmembrane regions of L-selectin were examined. ITC was used to determine binding affinities as well as other thermodynamic parameters for the interactions between both Ca^{2+}-free and Ca^{2+}-bound CaM and two peptides: one encompassing solely the cytoplasmic tail of L-selectin (LSEL*s*) and the second the cytoplasmic tail plus a seg-

ment of L-selectin thought to reside in the transmembrane domain (LSEL*l*) (Fig. 1*A*). Four different titrations were performed: LSEL*l* or LSEL*s* into Ca^{2+}-CaM and LSEL*l* or LSEL*s* into apo-CaM (Fig. 1*B*). From these titrations, the requirement for Ca^{2+} as well as a portion of L-selectin predicted to be in the membrane-spanning region becomes apparent. The binding curve of LSEL*l* with Ca^{2+}-CaM is characterized by a two-step process, similar to that reported for other CaM-binding peptides (32, 33). The first, which describes the binding of the first peptide to CaM, has a dissociation constant (K_d) on the order of 10^{-9} M and is driven predominantly by entropic factors (Fig. 1*C* and supplemental Table S1). The second step, corresponding to the binding of a second LSEL*l* peptide to Ca^{2+}-CaM, has a K_d on the order of 10^{-6} M, indicating a significantly weaker affinity, and is an enthalpically favorable event. Interestingly, despite different energetic driving factors and affinities, both LSEL*l* binding sites on Ca^{2+}-CaM are insensitive to an increased salt concentration, suggesting that these interactions are predominantly hydrophobic and are not driven by charge-charge interactions (supplemental Table S1). The occurrence of two binding events is supported by surface plasmon resonance experiments (data not shown). The titration of LSEL*l* into apo-CaM produced a complex endothermic binding curve with multiple LSEL*l* peptides interacting with CaM. Unlike the titration with the Ca^{2+}-bound protein, however, the number and identity of the thermodynamic interactions are not clear. Modeling of these data was largely unsuccessful, although a dissociation constant on the order of 10^{-6} M obtained for the first binding event is not unreasonable (data not shown). The results for LSEL*l* are contrasted with those for LSEL*s*. No significant amount of heat was released or absorbed from the titration of either Ca^{2+}-bound or -free CaM with this peptide that represents solely the cytoplasmic tail of L-selectin.

A similar outcome was seen when the interactions of both Ca^{2+}-bound and apo-CaM with the L-selectin peptides were examined through ^{15}N HSQC titrations, a technique that provides information on ligand-induced global conformational shifts as well as chemical exchange. A ^{15}N HSQC titration again points to two independent LSEL*l* binding sites on Ca^{2+}-CaM that differ significantly in affinity (supplemental Fig. S2*A*). Up until the 1:1 stoichiometric ratio, this titration is characterized by slow chemical exchange as the $^{1}H(N)$ backbone resonances corresponding to free Ca^{2+}-CaM disappear and those for complexed CaM appear. In contrast, the binding of the second LSEL*l* peptide to Ca^{2+}-CaM leads to broadening of the $^{1}H(N)$ resonances often to the point of disappearance. This effect is characteristic of intermediate chemical exchange on the NMR time scale and indicates a significantly weaker equilibrium constant for this interaction. Because slow exchange typically corresponds to an intermolecular dissociation constant on the order of 10^{-7} M or less and intermediate exchange often occurs when K_d is ~10^{-6} M, the type of chemical exchange observed for each of the binding events corresponds with the Ca^{2+}-CaM·LSEL*l* affinities obtained through calorimetry. Spectra characteristic of an intermolecular interaction in fast exchange on the NMR time scale were produced with the titration of LSEL*l* into apo-CaM as well as LSEL*s* into either Ca^{2+}- or apo-CaM; the observed backbone $^{1}H(N)$ resonances are an average
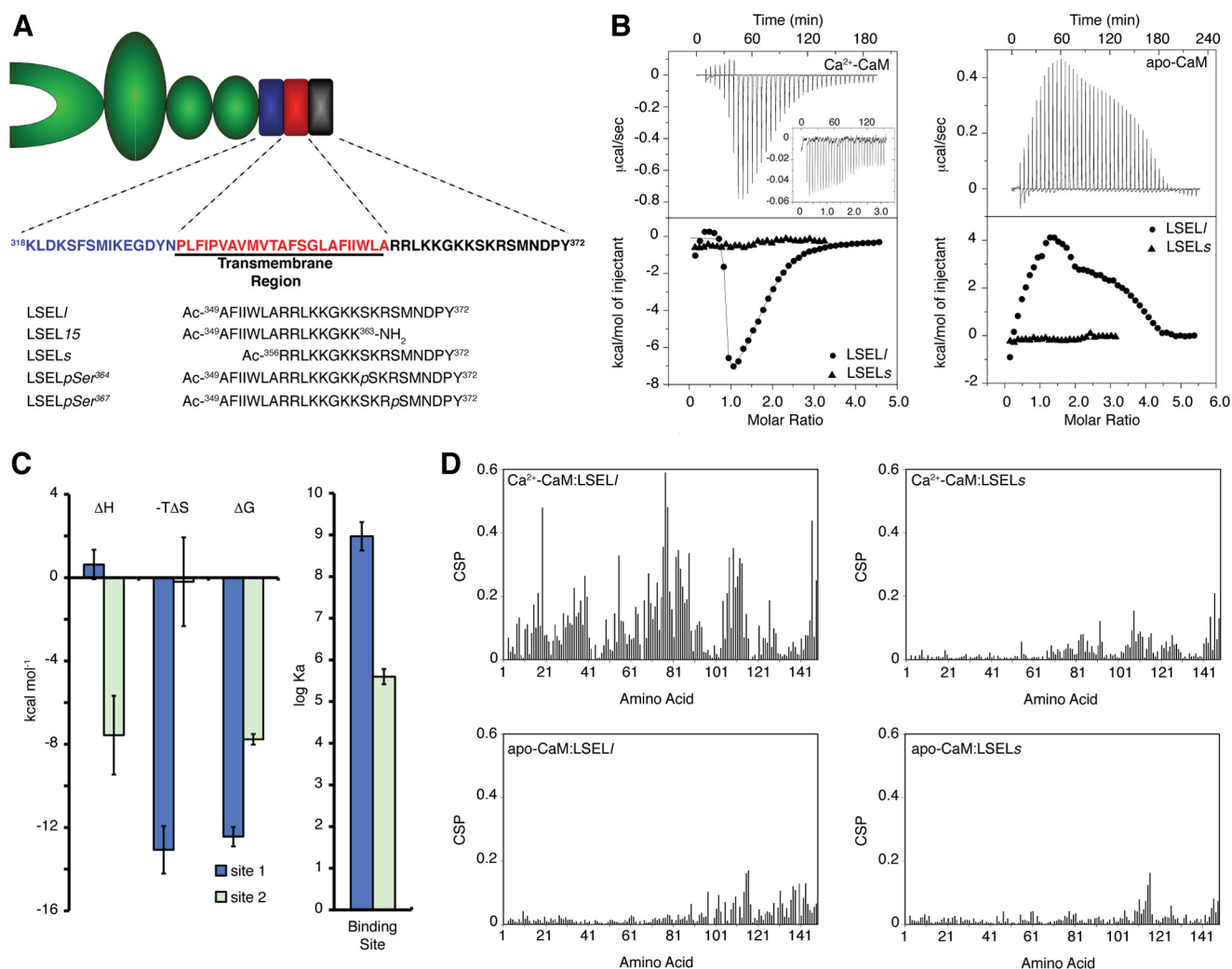
FIGURE 1. **Ca^{2+} dependence and role of the transmembrane helix in the interaction between CaM and L-selectin.** *A*, schematic of L-selectin with the membrane-proximal, transmembrane, and cytoplasmic domains *highlighted*. The four extracellular domains are shown in *green* and include (from *left* to *right*) a carbohydrate-binding lectin domain, an epidermal growth factor domain, and two short consensus repeat domains. The extracellular membrane-proximal region is indicated in *blue*, the single transmembrane helix is in *red*, and the cytoplasmic region is in *black*. The peptide sequences used in this study are placed at the *bottom*. *B*, calorimetric titration of Ca^{2+}-CaM or apo-CaM with LSEL*l* and LSEL*s* peptides. *Top panels*, base line-corrected raw ITC titration of LSEL*l* or LSEL*s* (*inset*) into either Ca^{2+}-CaM or apo-CaM. *Bottom panels*, overlay of the derived binding isotherms for the titration of LSEL*l* and LSEL*s* into either Ca^{2+}-CaM or apo-CaM. *C*, thermodynamic parameters of the calorimetric titration of Ca^{2+}-CaM with LSEL*l* displayed as *bars*. Error bars, S.E. for three independent experiments. Apparent are the different energetic driving factors and the significant difference in affinity between the two peptide binding events. *D*, backbone H$_N$ and N CSPs induced upon binding of either LSEL*l* or LSEL*s* to Ca^{2+}- or apo-CaM are plotted as a function of CaM amino acid residue.

of the free CaM and complexed CaM chemical shifts (supplemental Fig. S2, *B–D*). Fast chemical exchange is typically observed for intermolecular interactions with a dissociation constant on the order of 10^{-5} M or higher. Surface plasmon resonance experiments support an affinity of this magnitude for the binding of LSEL*s* to Ca^{2+}-CaM (data not shown).

Next, backbone CSPs were measured to characterize the regions of both apo- and Ca^{2+}-CaM affected by the addition of either LSEL*l* or LSEL*s* to the sample. The CSPs were then plotted as a function of residue number for the various CaM and peptide combinations (Fig. 1*D*). In agreement with the ITC results, the degree and extent of the CSPs observed was the most significant for the complex between Ca^{2+}-CaM and LSEL*l*. This combination exhibited significant chemical shift changes throughout CaM with the greatest extent observed in the central linker, a trend seen in other Ca^{2+}-CaM complexes (34). In contrast, the other combinations produced CSPs of a much smaller magnitude and located predominantly in the C-terminal lobe of CaM. Unlike the CSPs measured for Ca^{2+}-CaM·LSEL*l*, which represent the 1:1 complex, the CSPs for Ca^{2+}-CaM·LSEL*s*, apo-CaM·LSEL*l*, and apo-CaM·LSEL*s* were derived from peptide-saturated complexes.

Taken together, the biophysical data for this interaction highlight the roles of Ca^{2+} and a portion of L-selectin's predicted membrane-spanning region in creating a significant interaction between CaM and this protein. Although binding between CaM and L-selectin was detected in the absence of Ca^{2+} or with solely the cytoplasmic tail (using apo-CaM or LSEL*s*, respectively) these interactions are in fast exchange on the NMR time scale, produce small and localized CSPs in the CaM backbone ^{1}H(N) resonances, and either release/absorb very little heat as detected by ITC or suggest nonspecific binding. These observations are characteristic of significantly weaker interactions that are electrostatically driven. As such,

we suspect that the interaction between Ca^{2+}-CaM and LSEL*l* is the functionally important form of this complex.

Structure Determination of Ca^{2+}-CaM Complexed 1:1 with L-selectin—To understand the interaction between CaM and L-selectin at the molecular level, a solution NMR-based structure determination of Ca^{2+}-CaM bound 1:1 with LSEL*l* was carried out. Standard NMR-based structure determination of protein complexes proceeds via a series of experiments that first assign the resonances of CaM and the bound peptide and then independently determine the secondary and tertiary structures of CaM and the peptide through NOE-based distance restraints and finally solve the complex through the collection and analysis of intermolecular NOEs between CaM and the peptide. However, due to peak broadening observed even for the 1:1 complex between Ca^{2+}-CaM and LSEL*l*, this method was not viable. Instead, a reduced structure determination protocol was employed, in which the importance of methionine and the role that it plays in Ca^{2+}-CaM·target interactions is exploited and combined with the use of backbone RDCs to solve the structure of the CaM·L-selectin complex (15).

A comparison of solved CaM·target peptide structures reveals that it is through variation in domain orientation and not in backbone conformation that CaM binds its numerous targets (23). Consequently, RDC analysis can be used to determine the orientation of the two lobes of CaM when bound to LSEL*l* and provide a homologous starting model for the structure of CaM in the complex (18, 35). Because RDCs are a function of bond vector orientation in relation to the external magnetic field, they are particularly useful for orienting two domains of a protein with respect to each other (36). Here, the correlations between measured H_N-N RDCs for CaM bound to LSEL*l* and theoretical RDCs back-calculated from crystal structures deposited in the Protein Data Bank were determined (supplemental Table S2). The closest agreement obtained was to those back-calculated from the CaM·Ca(v)1.2 Ca^{2+} channel (Protein Data Bank code 2F3Y) (37). This published structure was subsequently used as the starting model for CaM in complex with L-selectin.

To facilitate the collection of NOE-based distance restraints required to determine the tertiary structure of the complex, the synthetic peptide employed was shortened from a 24-mer to a 15-mer. This peptide, LSEL*15*, bound to CaM in the same manner as LSEL*l* (Fig. 2, *A* and *B*, and supplemental Table S1) (results not shown) and produced spectra with narrower line widths, easing the process of resonance assignment. In total, 189 non-degenerate intrapeptide NOEs provided the distance restraints for calculation of the bound LSEL*15* structure by the automatic assignment and structure calculation program CYANA (version 2.0). The 20 lowest structures have a backbone RMSD of 0.71 Å (Fig. 2*C*). From the lowest energy structure, 171 distance restraints were supplied for the full complex structure calculation (Table 1).

The standard experiments used to assign the key aliphatic side chain methyls and collect intermolecular NOEs (a NOESY-^{13}C-^1H-HSQC and its F1-^{13}C,^{15}N isotope-filtered version, respectively) produced ambiguous resonance assignments and difficulties in assigning NOE cross-peaks. Unambiguous intermolecular NOEs are required to tie the complex together, pro-

viding distance restraints as well as domain translational information not supplied by RDCs. To solve this problem, a labeling scheme analogous to that of methyl-labeling isoleucine, leucine, and valine against a perdeuterated background was employed (38). Using CaM ^1H/^{13}C-labeled on the methyl groups of methionine but otherwise isotopically ^2H and ^{12}C ((^1H/^{13}C-*methyl*-Met)/^2H/^{15}N-labeled CaM), the high number of methionine residues in CaM (9 of 148 amino acid residues) and their location in the hydrophobic pockets were exploited to collect intermolecular NOEs between CaM and the bound peptide (15, 39). Altogether, 69 intermolecular NOEs between CaM and LSEL*15* as well as six intermethionine NOEs were measured (Fig. 2, *D* and *E*, and Table 1).

The solution structure of the 1:1 interaction between Ca^{2+}-CaM and LSEL*15* was calculated using a two-step, low temperature torsion angle simulated annealing protocol (15, 26). In this protocol, the RDC-selected homologous CaM starting structure was refined using backbone H_N-N RDCs and experimentally determined dihedral angle restraints, peptide-specific CYANA-derived distance and dihedral angle restraints, hydrogen bonding restraints for both molecules, and intermolecular NOEs (Table 1). The 30 lowest energy structures calculated in this manner have a backbone and heavy atom RMSD in the folded regions of 0.318 and 0.378 Å, respectively.

Solution Structure of Ca^{2+}-CaM Complexed 1:1 with the LSEL15 Peptide and Comparison with Other Complexes—The lowest energy solution structure of the 1:1 complex of Ca^{2+}-CaM·LSEL*15* is presented in Fig. 3*A*. The bound peptide is α-helical over almost its entire length (Phe[350]–Lys[362]), retaining the conformation calculated by CYANA (Fig. 2*C*). The N- and C-terminal lobes of CaM interact with the N- and C-terminal portions of the LSEL*15* peptide, respectively, to form a complex in parallel orientation relative to the bound peptide. The aliphatic side chain of LSEL*15* residue Ile[352] projects into the methionine-lined hydrophobic pocket of the N-lobe of CaM, anchoring the N-terminal portion of the peptide to this lobe of CaM (Fig. 3, *B* and *C*). In an analogous manner, the side chains of both Leu[354] and Leu[358] point into the hydrophobic pocket of the C-terminal lobe of CaM, anchoring the C-terminal portion of the peptide through a "double-anchor" motif (40). For all three key residues, a significant number of NOEs were collected between their side chains and the methionine probes that line the hydrophobic pockets of CaM. The basic residues downstream from Leu[358] interact with the exit channel of the C-terminal lobe of CaM. This channel is more negatively charged than the entrance channel formed by the CaM N-terminal lobe; thus, the parallel orientation observed is energetically favorable because the more hydrophobic or more positively charged halves of the peptide interact with the corresponding lobes of CaM. The combination of hydrophobic and electrostatic interactions between CaM and LSEL*15* probably explains the apparent insensitivity of this complex to increased salt concentration (supplemental Table S1).

Due to the spacing of the peptide anchors, the LSEL*15* peptide binds Ca^{2+}-CaM with a "1–3/7" motif. Although this particular spacing is novel, the motif is a hybrid of the 1–3 and 1–7 anchor positions seen in the MARCKS and NMDA receptor Ca^{2+}-CaM complexes, respectively (Protein Data Bank codes
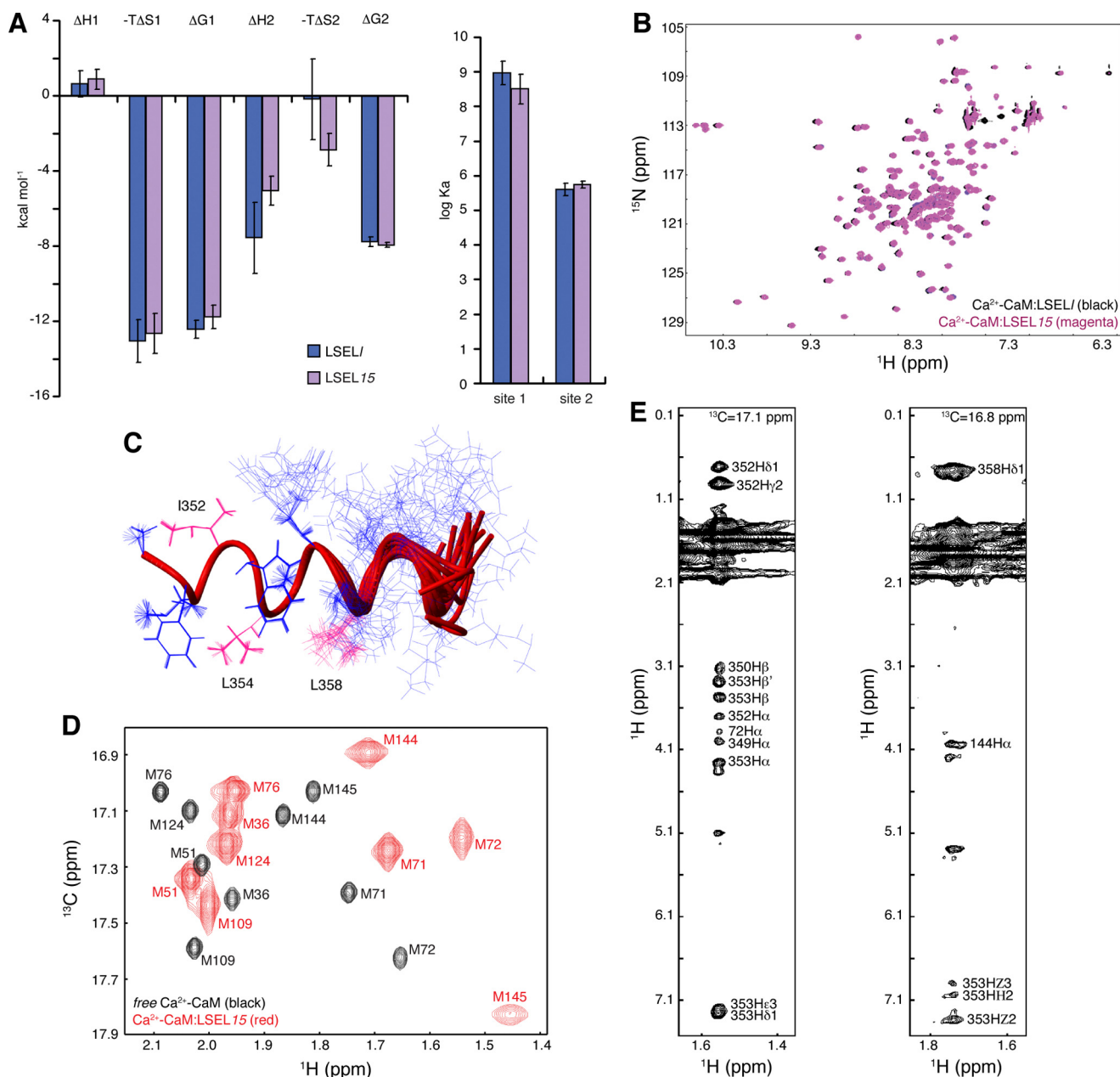
FIGURE 2. **NMR-based structure determination of 1:1 Ca²⁺-CaM·L-selectin complex.** *A*, bar graph comparing the determined thermodynamic parameters for the calorimetric titration of Ca²⁺-CaM with LSEL*l* or LSEL*15*. Data are represented as mean ± S.E. (*error bars*) for three independent experiments. *B*, overlays of ¹⁵N HSQC spectra of Ca²⁺-CaM complexed 1:1 with LSEL*l* and LSEL*15*. *C*, NOE-based solution structure of LSEL*15* when bound to Ca²⁺-CaM. The final 20 structures generated by CYANA (version 2.0) are aligned over residues 350–356. LSEL*15* is an α-helix from Phe³⁵⁰ to Arg³⁵⁶ in all 20 structures and from Phe³⁵⁰ to Lys³⁶² in the lowest energy structure. The anchor residues of Ile³⁵², Leu³⁵⁴, and Leu³⁵⁸ are indicated in *hot pink*. *D*, ¹³C HSQC spectrum of Ca²⁺-bound (¹H/¹³C-*methyl*-Met)/²H/¹⁵N-labeled CaM either peptide-free or complexed 1:1 with LSEL*15*. Due to the selective labeling scheme, only the methyl groups of the CaM methionines are detected. Eight of the nine methionine amino acid residues of CaM line the hydrophobic binding pockets of CaM, and changes in both line width and chemical shift of the methyl group of these residues point to the involvement of both lobes in the interaction with LSEL*15*. *E*, representative strip plots from ¹³C-edited NOESY-HSQC spectra of the 1:1 complex of (¹H/¹³C-*methyl*-Met)/²H/¹⁵N-labeled CaM and LSEL*15*. The intermolecular NOEs between the methyl groups of Met-72 (*left*) and Met-144 (*right*) and identified protons on LSEL*15* are indicated. Also seen are intramethionine NOEs between the Hε and Hα protons.

1IWQ and 2HQW). Counterintuitively, the side chain of Trp³⁵³ does not seem to serve as an anchor residue for either lobe of CaM and instead resides between them near the central linker (Fig. 3*A*), a position supported by fluorescence spectroscopy studies using selenomethionine-substituted CaMs (results not shown) (41). In comparison with the canonical 1–14 spacing seen for CaM bound to the myosin light chain kinase peptides, this 1–3/7 anchor spacing is much tighter, the consequence of

which is seen in the close proximity of the two lobes of CaM. If this proximity is measured as the distance between the centers of mass for each lobe, the LSEL*15* complex is more compact not just compared with myosin light chain kinase or the other kinase complexes, but also more compact than the NMDA receptor or MARCKS complexes (19.7 Å *versus* 20.6 and 21.1 Å, respectively) (supplemental Table S3). The entire backbone RMSD of Ca²⁺-CaM·LSEL*15* is quite large when compared

TABLE 1

Experimental restraints and structural statistics of the lowest energy structure of Ca^{2+}-CaM·LSEL*15*

Parameters	Values
No. of experimental restraints	
Distance restraints from NOEs	
CYANA-derived intrapeptide upper distance restraints	171
CaM intermethionine NOEs	6
Intermolecular NOEs	69
H_N-N RDC restraints	109
Backbone dihedral angle restraints	
CaM[a]	288
LSEL*15*[b]	28
Hydrogen bonding restraints	
CaM[c]	116
LSEL*15*[d]	6
Ca^{2+} chelation restraints	24
Average RMSD values from experimental data	
Distance restraint violation (Å)	0.082
Dihedral angle restraint violation (degrees)	2.341
RDC restraint violation (Hz)	0.092
Average RMSD values from idealized covalent geometry	
Bonds (Å)	0.003
Angles (degrees)	0.422
Impropers (degrees)	0.345
Ramachandran analysis of Ca^{2+}-CaM·LSEL*15*[e]	
Residues in favored regions (%)	94.8
Residues in additionally allowed regions (%)	5.2
Residues in generously allowed regions (%)	0
Residues in disallowed regions (%)	0

[a] Predicted from TALOS (25).
[b] Obtained from the lowest-energy bound LSEL*15* structure calculated by CYANA-2.0.
[c] Based on CSI-defined secondary structure.
[d] Based on secondary structural elements common to the 20 lowest energy structures of bound LSEL*15* calculated by CYANA-2.0.
[e] Performed using PROCHECK on structure regions 6–144 and 350–362.

with other known structures; however, on a domain by domain basis, this difference is much smaller, and the tertiary structure is in quite good agreement, reflecting the versatility of the flexible linker in accommodating widely different CaM-binding domains.

Molecular Model for the Simultaneous, Non-competitive Binding of CaM and Ezrin/Moesin FERM Domain to the Tail of L-selectin—In addition to and concurrent with CaM, members of the ERM family of membrane-cytoskeleton cross-linkers bind the cytoplasmic tail of L-selectin. By linking L-selectin's cytoplasmic tail with the actin cytoskeleton, the ERM family is thought to distribute L-selectin to the tips of microvilli, facilitating leukocyte tethering under flow, and play a role in phorbol 12-myristate 13-acetate-induced shedding (42, 43). The binding sites for CaM and the FERM domain of ezrin/moesin are thought to overlap, and both *in vitro* and *in vivo* evidence suggests that FERM and CaM are able to bind to non-competing regions of the same tail, forming a 1:1:1 heterotrimeric complex in the unactivated cell (30). Due to the "tight quarters" in this juxtamembrane region, the compact nature of the CaM domain orientation in our 1:1 Ca^{2+}-CaM·LSEL*15* structure would help facilitate the binding of an ERM family member to L-selectin. Indeed, several C-terminal residues of LSEL*15* remain exposed to the solvent, including Arg[357] and Lys[362], which have been identified as critical for the interaction with moesin-FERM (Fig. 4*A*) (42, 44).

Using our determined solution structure of the CaM·L-selectin interaction, we have been able to build upon an existing model of the heterotrimeric complex (30) (Fig. 4*B* and supple-

mental Fig. S1). Because the molecular model created by Killock *et al.* (30) had undergone extensive energy minimization and dynamics cycles, the atomic positions of moesin FERM and amino acid residues Ser[364] to Tyr[372] of L-selectin from this model were combined with those of CaM and L-selectin residues Ala[349] to Lys[363] from the CaM·LSEL*15* complex and aligned using the L-selectin residues common to both structures (Arg[356]–Lys[363]) to orientate the individual components. The generated model produces a clearer picture of the heterotrimeric interaction because the structure of L-selectin bound to CaM as well as the positioning of CaM in relation to L-selectin is experimentally determined rather than modeled. Not only does this model provide a visual representation of how CaM and ERM could both bind non-competitively to the cytoplasmic tail of L-selectin, but because a significant amount of the C-terminal region of the tail remains solvent-exposed (Fig. 4*C*), it also provides structural plausibility for the binding of additional cytoplasmic partners, such as α-actinin and PKC isozymes. In the model, the C-terminal L-selectin amino acid residues that extend beyond those represented by the LSEL*15* peptide and thus without an experimentally determined position (Ser[364]–Tyr[372]) are represented as a random coil, a secondary structure supported by NMR-based experiments using the bound LSEL*l* peptide (results not shown).

Phosphorylation of the L-selectin Tail Does Not Directly Regulate the Interaction with CaM—It has been proposed that for L-selectin, as for many other proteins, the PKC phosphorylation and CaM-binding sites overlap and that phosphorylation of serine residues in L-selectin's cytoplasmic tail by PKC leads to disassociation of CaM and thus shedding of the extracellular domains (11, 12). GPCR stimulation activates PKC pathways, and in phorbol ester- or chemoattractant-activated leukocytes, PKC isozymes have been found interacting with the L-selectin tail, and this sequence is phosphorylated on evolutionarily conserved serine residues (Ser[364] or Ser[367]) (Fig. 5*A*) (5). However, binding studies performed through both ITC and ^{15}N HSQC titrations indicate that phosphorylation on these residues does not impede the ability of CaM to bind L-selectin (Fig. 5*B*, supplemental Fig. S3, and supplemental Table S1). This observed insensitivity to phosphorylation agrees with our presented structural data on the 1:1 CaM·L-selectin complex because both Ser[364] and Ser[367] are outside of L-selectin's CaM-binding domain. Instead, our model of the heterotrimeric complex suggests that phosphorylation could affect the interaction between L-selectin and the N-terminal domain of ezrin/moesin. Both Ser[364] and Ser[367] are close to and involved in the interaction with moesin (Fig. 5*C*), and phosphorylation on either residue could lead to a change in the ability of ezrin/moesin to bind L-selectin and indirectly influence CaM binding.

Structural Characterization of the 1:2 Ca^{2+}-CaM·LSEL15 Interaction—Due to significant peak broadening observed upon the addition of a second molar equivalent of LSEL*l* or LSEL*15* to Ca^{2+}-CaM (supplemental Fig. S2), the 1:2 complex is not amenable to NMR-based structure determination. However, on the basis of observed signal broadening in ^{15}N HSQC spectra, we have determined regions of Ca^{2+}-CaM affected by the interaction with the second LSEL*l/15* peptide. The broadening of backbone cross-peak signals in ^{15}N HSQC spectra of
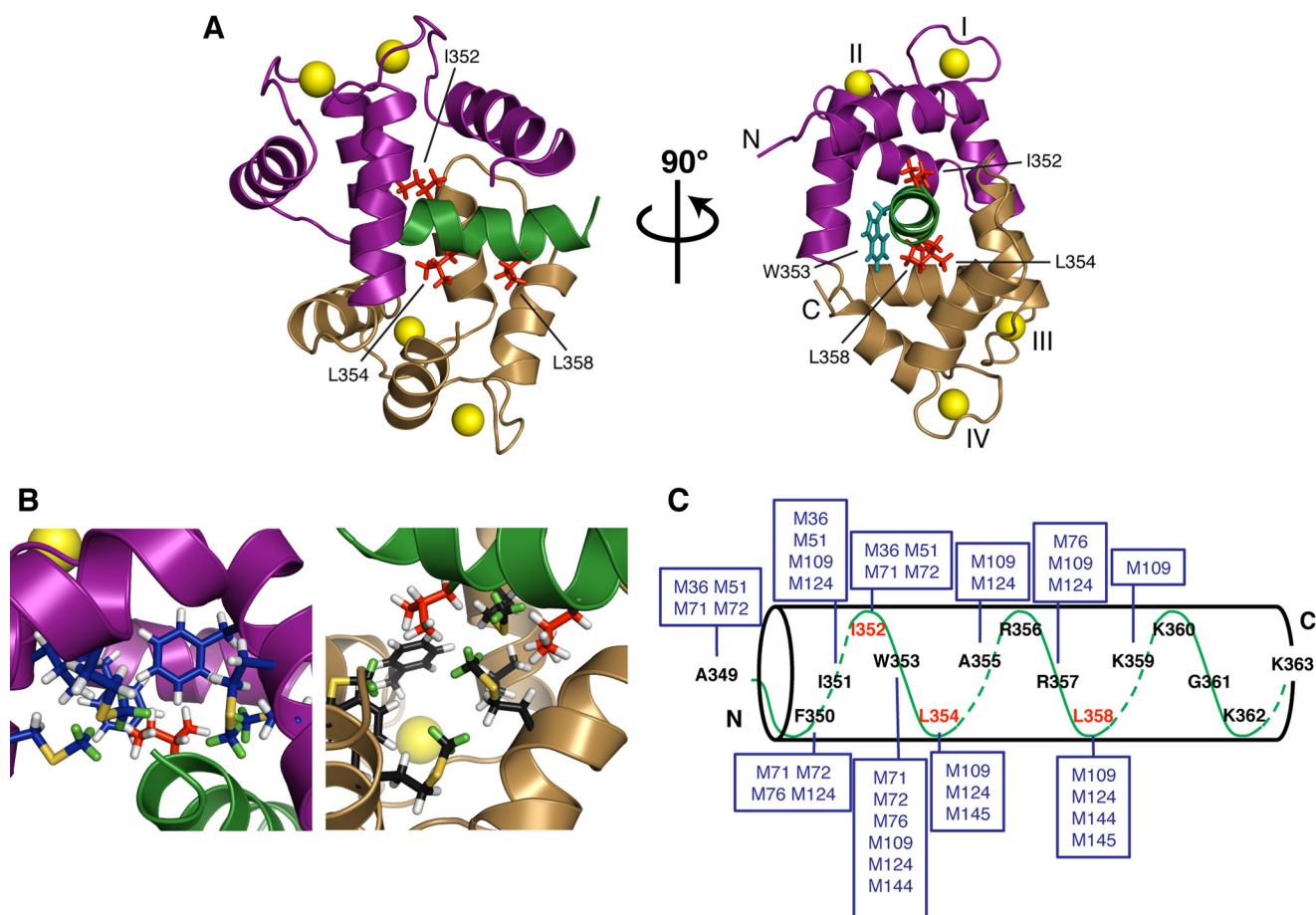
FIGURE 3. **Structural basis for the 1:1 interaction of Ca^{2+}-CaM with L-selectin.** *A, ribbon representation* of the lowest energy structure of the complex. The N- and C-terminal lobes of CaM are shown in *purple* and *gold*, respectively, and the LSEL*15* peptide is indicated in *green*. The side chains of LSEL*15* amino acid residues Ile[352], Leu[354], and Leu[358] are *highlighted* in *red*. Together, these three side chains anchor the LSEL*15* peptide to CaM with a "1–3/7 motif." The side chain of Trp[353] is in *teal*. The four Ca^{2+} ions are indicated as *yellow spheres*. *B*, closer view of the interface between CaM and the anchoring amino acid side chains of LSEL*15*. *Right*, interaction of the CaM N-lobe with Ile[352] of LSEL*15*; *left*, interaction of the CaM C-lobe with Leu[354] and Leu[358] of LSEL*15*. In each *panel*, the helices and side chain carbons are *colored purple/navy*, *gold/black*, or *green/red* for the N- or C-lobe of CaM or LSEL*15*, respectively. Methionine methyl group protons that serve as probes for intermolecular NOEs between CaM and LSEL*15* are *colored green*. *C*, schematic showing the observed intermolecular NOEs between the methionine methyl groups of CaM (*boxed*) and the LSEL*15* peptide. Key interacting residues Ile[352], Leu[354], and Leu[358] of LSEL*15* are indicated in *red*.

peptide-saturated Ca^{2+}-CaM (a 1:2.5 molar ratio) is not uniform, and analysis of normalized peak height (peak height as it compares to that in the 1:1 spectra) can quantify the degree of signal loss on a per residue basis (Fig. 6*A* and supplemental Fig. S2*A*). Many ^{15}N HSQC cross-peaks originating from backbone resonances in the second and third EF-hands as well as the central linker are broadened to the extent that they have disappeared (0% normalized peak height). As mentioned earlier, this observation is characteristic of an intermediate exchange regime and suggests that these residues are participating in a medium strength interaction. When the degree of signal loss is mapped onto the 1:1 structure of Ca^{2+}-CaM·LSEL*15*, those residues most affected by the binding of the second peptide suggest a secondary interface on the top of the CaM molecule away from the Ca^{2+}-binding EF-loops (Fig. 6*B*). This secondary interface is made up of a negatively charged face on the CaM C-lobe and a hydrophobic groove found on the back of the N-lobe. It is conceivable that the more hydrophobic portion of LSEL*15* or LSEL*l* could bind to the groove while the positively charge sequences of these peptides bind the negative face. Although this second binding site involves both lobes of CaM, it

is distinct from the hydrophobic pockets that create the "classical" Ca^{2+}-CaM binding site through which the first LSEL*l*/*15* peptide interacts.

DISCUSSION

The presented study examines at a biophysical and structural level the interaction between CaM and L-selectin. We have determined the solution structure of Ca^{2+}-CaM bound 1:1 to a synthetic peptide representing the cytoplasmic/transmembrane domain of L-selectin. Due to broad and missing signals, particularly from critical side chain methyl groups, initial attempts to determine a high resolution structure of this complex through a traditional NOE-based strategy were unsuccessful. Therefore, a novel structure determination protocol was employed in which backbone H_N-N RDCs were used to determine the domain orientation of the two lobes of CaM, and intermolecular NOEs between the CaM methionine methyl groups and the protonated peptide defined how the orientated domains bind the peptide. This structure explains the requirement for both Ca^{2+} and the putative transmembrane region of L-selectin in forming a strong interaction between these two
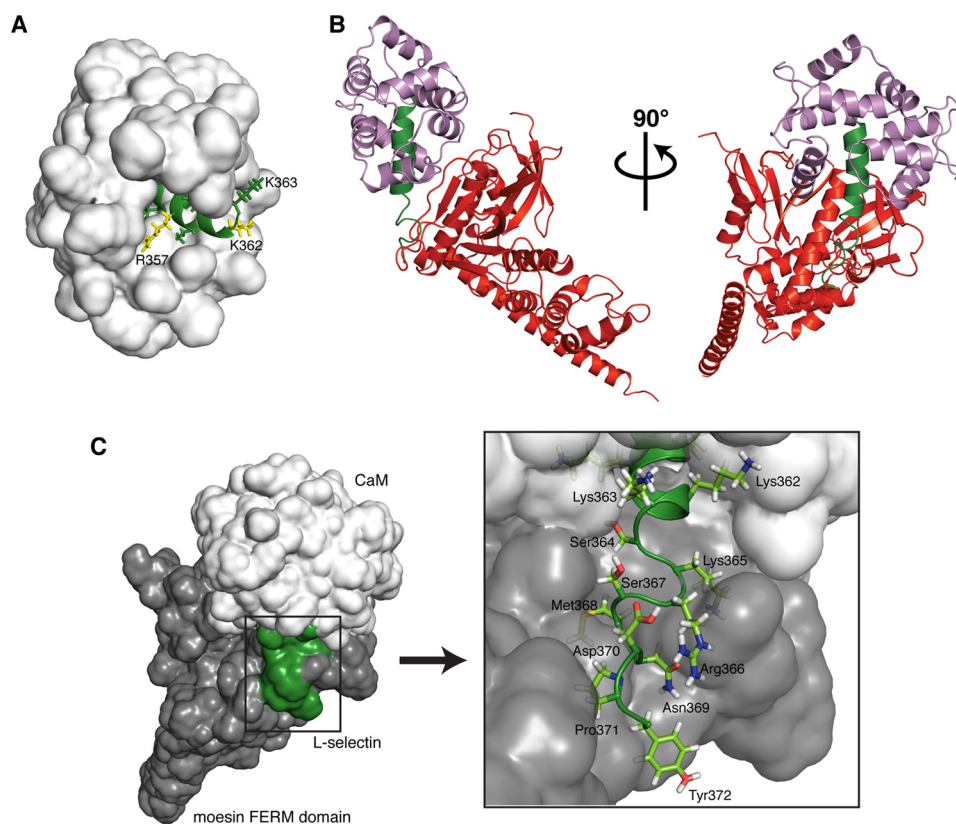
FIGURE 4. **Structural model of the CaM·L-selectin·ERM heterotrimeric complex.** *A*, the close positioning of the two lobes of CaM when bound to LSEL*15* enables the C-terminal residues of LSEL*15* implicated in the interaction with FERM to be solvent-exposed. The solvent-accessible surface area of CaM is shown in a *white surface representation*; bound LSEL*15* is shown as a *green ribbon*, and the solvent-exposed side chains of L-selectin are shown in *green*, with those thought to be involved in the interaction with FERM *highlighted* in *yellow*. *B*, heterotrimeric complex of CaM·L-selectin·ERM with the secondary structural elements colored as follows: CaM (*purple*), L-selectin (*green*), and moesin FERM (*red*). *C*, despite forming interactions with both CaM (*white*) and FERM (*gray*), a significant portion of the C-terminal region of L-selectin's tail (*green*) remains solvent-exposed. The solvent-accessible surface area of all three components is shown with atomistic detail of L-selectin's exposed C-terminal residues indicated (*box*).

proteins, as suggested by both ITC and CSPs (Fig. 1). It is through the hydrophobic patches exposed in the Ca^{2+}-replete state that the two lobes of CaM bind the hydrophobic side chain anchors of L-selectin (Fig. 3). Two of these anchors, Ile^{352} and Leu^{354}, are located in the predicted membrane-spanning region of L-selectin (the third, Leu^{358}, is in the established cytoplasmic tail), indicating that CaM must either pull this region out of the membrane, perturb the membrane bilayer structure, or do a combination of both to bind L-selectin (discussed below).

At the physiological level, the requirement for Ca^{2+} is a bit unexpected. The interaction between CaM and L-selectin is thought to exist in resting leukocytes, a state in which the cytoplasmic Ca^{2+} concentration is 10^{-7} M and CaM is in either an apo or partially Ca^{2+}-bound form. However, both the absence of the coimmunoprecipitation of CaM with L-selectin in the presence of the Ca^{2+}-chelator EDTA (12) and the directly induced shedding of L-selectin from both neutrophils and lymphocytes upon the addition of pharmacological Ca^{2+}-CaM inhibitors (11) point to the *in vivo* Ca^{2+} requirement of this interaction. The contemporary belief in spatial/temporal aspects of Ca^{2+} signaling, conceptualized by microdomains, could help to explain this discrepancy. As Ca^{2+} enters the cytoplasm, it produces a local plume, a restricted domain of increased Ca^{2+} concentration that on its own or in combination to produce larger microdomains can regulate specific cel-

lular processes in different regions of the cell (45). The time scale of the Ca^{2+} influx is also critical because brief transients lead to a more restricted increase influencing effectors solely in the nearby environment, contrasting with the global concentration change and universal effector activation that results from a sustained influx. The engagement of ligands by L-selectin's lectin domain has been shown to cause an internal store-derived increase in cytosolic Ca^{2+} through a pathway independent of heterotrimeric G-proteins (46). However, the magnitude and duration of this Ca^{2+} influx is smaller and shorter than that seen with GPCR engagement. The Ca^{2+} "puffs" produced could lead to a concentration high enough to allow Ca^{2+}-CaM to bind L-selectin but localized and of a duration short enough to distinguish the effects from GPCR- or immunoreceptor-based cell activation characterized by a global Ca^{2+} increase that lasts for hours and triggers L-selectin ectodomain shedding (47, 48). Furthermore, CaM, like other members of the EF-hand superfamily, exhibits a strong increase in affinity for Ca^{2+} in the presence of a target protein (49). Therefore, it is reasonable to expect that in the presence of L-selectin, a significant portion of CaM may be Ca^{2+}-bound even at 100 nM Ca^{2+}, interacting with L-selectin in its Ca^{2+}-bound state in the resting cell.

The solution structure highlights the role of L-selectin's juxtamembrane region in the interaction between L-selectin and CaM; the C-lobe of CaM binds predominantly to this sequence
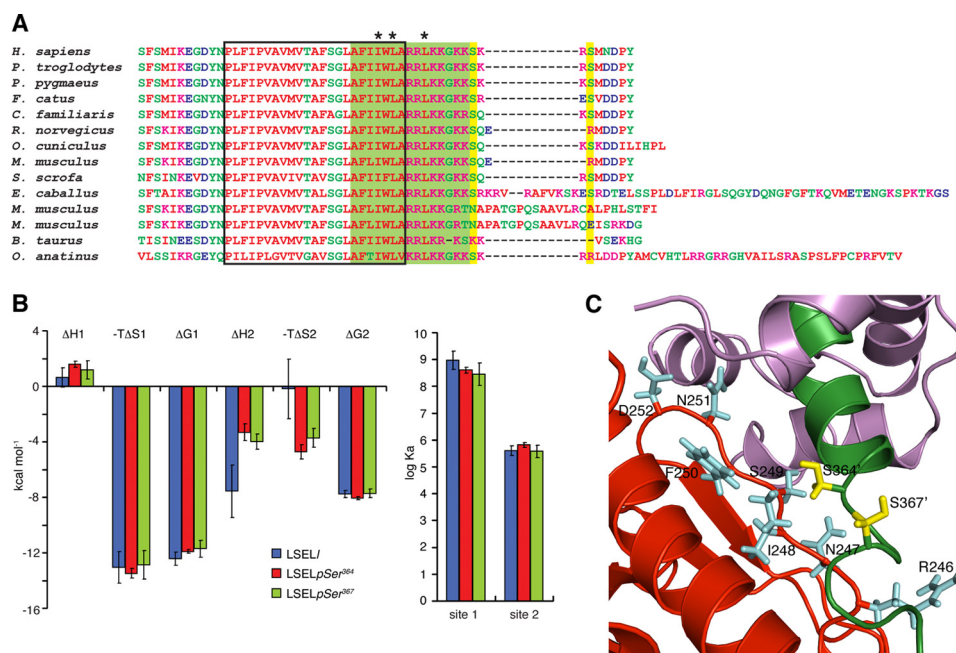
FIGURE 5. **Phosphorylation of the L-selectin tail does not induce CaM dissociation.** *A*, sequence alignment of the membrane-proximal, transmembrane, and cytoplasmic domains of mammalian L-selectins performed using ClustalW (74). The predicted transmembrane domain, region encompassed by the LSEL*15* peptide, and predicated PKC phosphorylation sites are delineated by a *black box*, *filled green box*, and *filled yellow boxes*, respectively. *, LSEL*15* anchor residues for the interaction with Ca^{2+}-CaM. *B*, thermodynamic parameters of the calorimetric titration of Ca^{2+}-CaM with LSEL*l*, LSEL*pSer^{364}*, or LSEL*pSer^{367}* displayed as *bars*. Data are represented as mean ± S.E. (*error bars*) for three independent experiments. Apparent is the insensitivity of CaM to the phosphorylation state of L-selectin. *C*, *close-up view* of the interface of L-selectin and moesin FERM with the same secondary structure *coloring scheme* as in Fig. 4*B*. The side chains of L-selectin residues Ser^{364} and Ser^{367} are indicated in *yellow*, whereas side chains of moesin residues at the interface are indicated in *light blue*. Both serines are close to the binding interface, in particular Ser^{364}, which appears to interact with Ile^{248} of moesin.

that includes the anchor residue Leu^{358}. This finding is supported by both *in vitro* and *in vivo* experiments. Coimmunoprecipitation studies with either mapping antibodies or truncation mutants indicate that the eight C-terminal amino acids of the tail are not required for binding (11, 12), a fact mirrored in the similar CaM-binding abilities of the LSEL*l* and LSEL*15* peptides (Fig. 2 and supplemental Table S1). *In vitro* peptide binding array and *in vivo* mutant-based shedding studies as well as L-selectin splice variants found in mice further define cytoplasmic amino acid residues ^{356}RRLKKG^{361} as critical to CaM binding (Fig. 5*A*) (12, 13, 50, 51). Coimmunoprecipitation experiments on transfected L-selectin mutants support the role of Leu^{358} and Lys^{359} in anchoring the C-lobe of CaM and forming favorable interactions with this lobe's negatively charged exit channel, respectively (11).

Due to large degrees of error associated with the derived constants and related to the small magnitude of the observed enthalpy change (the data are significantly scattered off the smooth theoretical curve), we did not report curve fitting of the ITC data for the binding of LSEL*s* to CaM (Fig. 1*B*); however, an affinity on the order of 10^{-5} M was obtained using surface plasmon resonance (data not shown). A recent publication by Deng *et al.* reported a dissociation constant on the order of 10^{-6} M for the interaction between CaM and the cytoplasmic tail of L-selectin (52). This value, similar for both Ca^{2+}- and apo-CaM, was determined using ITC and a peptide representing the cytoplasmic domain plus one amino acid of the putative transmembrane helix (L-selectin residues Ala^{355}–Tyr^{372}). Both the peptide studied by Deng *et al.* (52) and LSEL*s* exhibit an exothermic enthalpy change of similar magnitude upon binding CaM; however, differences in chemical exchange behavior suggest that the peptide studied by Deng *et al.* binds CaM with higher affinity than our peptide LSEL*s*; the binding between LSEL*s* and CaM occurs in fast chemical exchange on the NMR time scale (supplemental Fig. S2), whereas the peptide studied by Deng *et al.* (52) bound in intermediate exchange. The addition of hydrophobic Ala^{355} to the cytoplasmic domain peptide most likely explains the difference in affinity and exchange behavior of the two peptides.

Despite significant research focused on the ability of L-selectin's cytoplasmic juxtamembrane region to bind CaM, the predicted membrane-spanning region has largely been ignored, and yet the presented study provides structural evidence that this sequence is critical for the interaction of these two proteins. Amino acid residues Ile^{352} and Leu^{354} that serve to anchor the N- and C-lobes of CaM originate in the first turn of the proposed transmembrane helix, and the neighboring bulky, hydrophobic amino acid residues found in this sequence of L-selectin form favorable interactions with the hydrophobic patches exposed in Ca^{2+}-CaM. It is likely that these hydrophobic patches create an environment of characteristics similar to those found in the membrane, a fact highlighted by the lipid binding abilities of CaM (23). *In vitro* support for this structure is provided by Deng *et al.* (52), who observed FRET between a fluorescence probe attached to CaM and Trp^{353} when a peptide representing the external cleavage site, transmembrane helix, and cytoplasmic domain of L-selectin was reconstituted in a phosphatidylcholine bilayer. The interaction of CaM with a sequence predicted to extend by ~6 amino acids into L-selectin's putative membrane-spanning region is not a unique
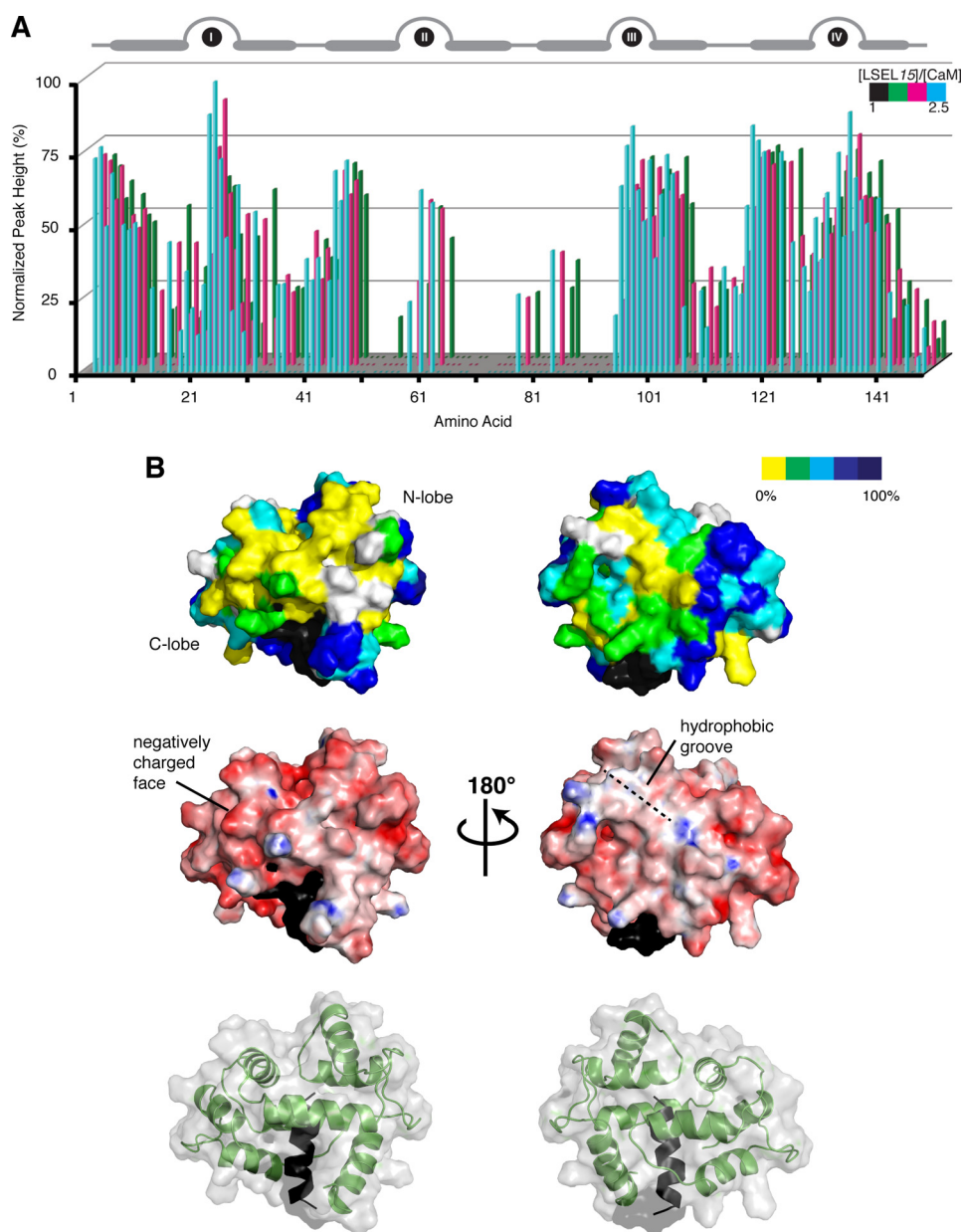
FIGURE 6. **Mapping the binding interface of the second LSEL15 peptide on the 1:1 Ca²⁺-CaM·LSEL15 complex.** *A*, NMR titration analysis of unlabeled LSEL15 binding to ¹⁵N-labeled Ca²⁺-CaM. ¹⁵N HSQC spectra of ¹⁵N-labeled CaM were collected at titration steps corresponding to [LSEL15]/[CaM] molar ratios of 1 (*black*, 100% peak height not shown), 1.5 (*green*), 2 (*magenta*), and 2.5 (*cyan*). Normalized peak heights of ¹⁵N-labeled CaM from the HSQC spectra are plotted against CaM residues. The position of the four EF-hands of CaM is indicated at the *top* of the diagram. *B*, surface representations of the 1:1 Ca²⁺-CaM·LSEL15 complex. *Top*, residues are *colored* according to their height in ¹⁵N HSQC spectra of the 2.5:1 [LSEL15]/[CaM] molar ratio, normalized against peak height in spectra of the 1:1 molar ratio. *Yellow*, missing; *green*, <30%; *cyan*, between 30 and 60%; *blue*, between 60 and 90%; *navy*, >90%. Residues not included in the analysis due to peak overlap are *colored white*, whereas those that correspond to that of the first LSEL15 peptide are *colored black*. The addition of a second LSEL15 peptide maps predominantly to the "top" of the CaM molecule. *Middle*, charged surface structure highlighting the acidic and basic side chains of CaM. The negatively charged face and hydrophobic groove thought to support the binding of the second LSEL15 peptide are shown. *Bottom*, *ribbon structure* displayed together with *surface structure* indicating the orientation of the 1:1 Ca²⁺-CaM·LSEL15 complex presented in the other two *panels*.

occurrence. Ca²⁺- and integrin-binding protein 1 binds the cytoplasmic tail of the α_{IIb} subunit of the platelet integrin $\alpha_{\text{IIb}}\beta_3$ through a sequence both juxtamembrane to and extending by six amino acids into the predicted membrane-spanning region (53–58). Furthermore, bioinformatic analysis presented here indicates that several other transmembrane receptors down-regulated through Ca²⁺/CaM-dependent ectodomain shedding have CaM-binding motifs that extend into the transmembrane domain (Fig. 7) (59–61). This suggests a common mode

of CaM-mediated regulation that, to date, has yet to be studied *in vivo*.

The CaM·L-selectin solution structure provides insight into a mechanism through which CaM regulates L-selectin ectodomain shedding. The interaction between the C-lobe of CaM and the cytoplasmic tail is driven through electrostatic forces, as suggested by the ITC and NMR titration data and by the fact that both apo- and Ca²⁺-CaM bind this region (Fig. 1D) (11, 30, 52). CaM would be electrostatically attracted to this part of
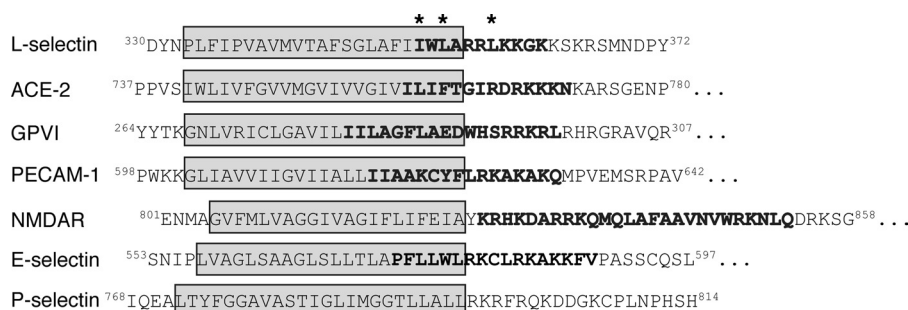
FIGURE 7. **Other transmembrane receptors down-regulated through Ca^{2+}-dependent ectodomain shedding have CaM-binding motifs extending into the transmembrane domain.** Analysis of L-selectin, angiotensin-converting enzyme 2 (ACE-2), platelet glycoprotein VI (GPVI), and platelet endothelial cell adhesion molecule 1 (PECAM-1) reveals the presence of CaM binding motifs proximal to and extending into the predicted membrane-spanning region (see the Cellular Calcium Information Server Web site) (75, 76). In contrast, the C0 CaM-binding domain from the NR1 subunit of *N*-methyl-D-aspartate receptor is located solely in the cytoplasmic domain. Like L-selectin, the cytoplasmic domain of E-selectin contains a putative CaM-binding domain, but whether or not CaM associates with this molecule is not well defined. P-selectin does not contain a putative CaM-binding domain. For each sequence, the transmembrane domain is *boxed* in *gray*, and the high scoring predicted CaM-binding region is indicated in *boldface type*. *, LSEL*15* anchor residues for the interaction with Ca^{2+}-CaM. Interestingly, ACE-2 could bind CaM with the same 1–3/7 spacing of L-selectin through amino acid residues Ile^{759}, Ile^{761}, and Ile^{765}.
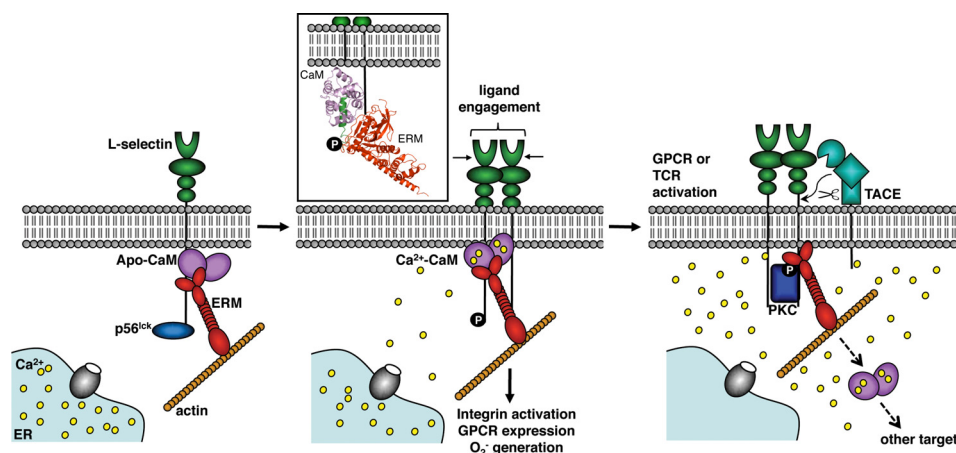
FIGURE 8. **Schematic of CaM-regulated L-selectin ectodomain shedding.** Pictured are suspected binding partners of the cytoplasmic tail of L-selectin in both the resting and activated leukocyte cell. In the resting cell, apo-CaM binds to the juxtamembrane region of L-selectin, a member of the ERM family connects L-selectin to the actin cytoskeleton, and p56^{lck}, an Src-tyrosine kinase, associates with the C-terminal end of the tail. Ligand engagement by L-selectin's lectin-binding domain induces clustering of the receptor, phosphorylation of Tyr^{372} by p56^{lck}, and the release of Ca^{2+} "puffs" from internal stores. The local increase in Ca^{2+} concentration enables CaM to bind L-selectin's anchor residues found both in the juxtamembrane region (Leu^{358}) and in the first turn of the proposed membrane-spanning domain (Ile^{352} and Leu^{354}). By potentially pulling this region out of the membrane, this binding interaction enacts a conformation change on the extracellular side of the plasma membrane that prevents the TACE protease from accessing the cleavage site. In the activated cell, a sustained, global increase in cytoplasmic Ca^{2+} concentration leads to CaM dissociation for other targets, such as calcineurin or the CaM-kinases, an act that releases the tail and exposes the cleavage site on the extracellular side of the membrane. Members of the ERM family continue to connect L-selectin to the actin cytoskeleton in the activated cell, potentially facilitating the co-localization of L-selectin with TACE to the cell's uropod. L-selectin is also phosphorylated by PKC isozymes, which may affect interaction with the ERM family or enable the interaction of additional binding partners.

L-selectin dangling down from the plasma membrane, and in the Ca^{2+}-bound state, it would bind both the positive charges and Leu^{358} found in the juxtamembrane region. The importance of this event is seen by the fact that CaM does not coimmunoprecipitate with L-selectin ^{358}LKK^{360}/^{358}EEE^{360} cytoplasmic or Arg^{356} truncation mutants (12). Once bound, due to the dynamic nature of the lipid membrane, CaM would "sense" anchor residues Ile^{352} and Leu^{354} present in the first helical turn of L-selectin's proposed membrane-spanning region. By binding these residues and their neighboring hydrophobic amino acids, CaM could effect a conformational change on the extracellular side of the membrane, preventing proteolytic cleavage. Upon cell activation, CaM disassociation would release this portion of L-selectin enacting a structural rearrangement, exposing the TACE cleavage site (Fig. 8).

This inside-out signaling hypothesis is supported by both *in vivo* and *in vitro* evidence. First, the sequence of L-selectin's transmembrane domain and juxtamembrane region is conserved throughout evolution (Fig. 5*A*). Second, considerably less CaM is associated with the 6-kDa trunk of L-selectin retained in the membrane following cleavage, pointing to its dissociation as a regulatory mechanism (12). Third, cytoplasmic mutations that abrogate the interaction with CaM affect the binding of an antibody against L-selectin's extracellular membrane-proximal cleavage site (11). This antibody can bind when CaM is bound to the cytoplasmic tail, suggesting that interacting partners of the cytoplasmic portion of L-selectin affect the conformation of its extracellular sequence. Finally, studies on L-selectin's membrane-proximal cut site point to the relaxed sequence specificity but length and conformational requirement of the TACE protease because both truncations as well as proline substitutions prevented proteolysis (51). It appears that a membrane-proximal stalk of sufficient length is required to permit TACE access to the substrate, and the bind-

ing of CaM to the cytoplasmic tail could cause a conformational change on the extracellular side of the membrane that shortens the amount of stalk available, preventing cleavage.

A key unanswered component of this proposed mechanism is the cause of CaM dissociation from the cytoplasmic tail of L-selectin. Our results suggest that the cause is neither a Ca^{2+}-induced conformational change in CaM nor, as has been widely speculated, phosphorylation of serine residues found in the cytoplasmic tail of L-selectin (Fig. 5, supplemental Fig. S3, and supplemental Table S1). Although ITC experiments indicate that L-selectin binds Ca^{2+}-CaM with an initial dissociation constant on the order of 10^{-9} M (supplemental Table S1), it is possible that the *in vivo* affinity is not as high due to other energetic considerations, such as potential membrane interactions and the presence of other proteins bound concurrently to the cytoplasmic tail. As a result, the sustained Ca^{2+} influx and resulting global concentration increase mediated by CRAC (calcium release-activated calcium) channels upon GPCR or immunoreceptor engagement may expose more abundant and higher affinity CaM binding sites, such as calcineurin and the CaM kinases, two families of proteins up-regulated upon cell activation. Alternatively, the induced close proximity of phosphatidylserine or phosphorylated phosphatidylinositols has been suggested to play a role in CaM disassociation (52).

Treatment of leukocytes with lineage-specific activating stimuli induces PKC-dependent phosphorylation of Ser^{364} and/or Ser^{367} in the cytoplasmic domain of L-selectin. The result of this phosphorylation is 2-fold. First, an increase in L-selectin's ligand binding activity is observed (62, 63). This response is immediate and preludes the ectodomain shedding of L-selectin that occurs minutes following cell activation. Second, mutagenesis-based studies have shown serine phosphorylation to be key to cell activation-linked ectodomain shedding (43). The introduction of one or two highly negatively charged groups significantly alters the local surface characteristics of that region of the protein, typically inducing or preventing intra- or intermolecular interactions. Because serine phosphorylation does not directly affect the ability of CaM to bind L-selectin (Fig. 5B, supplemental Fig. S3, and supplemental Table S1), it probably plays a role in the regulation of L-selectin's other cytoplasmic binding partners. Through both *in vitro* binding experiments and *in vivo* fluorescence lifetime imaging microscopy, members of the ERM family of cytoskeleton-membrane cross-linkers have been found to co-localize with CaM to the cytoplasmic domain of L-selectin (Fig. 4B) (30) and play a significant role in both tethering of the adhesion receptor to its ligands as well as in PKC-dependent shedding (64, 65). The side chains of both Ser^{364} and Ser^{367} (although to a lesser extent) are at the interface of the FERM domain of ezrin/moesin and L-selectin, and it is likely that their phosphorylation would affect this binding interaction (Figs. 4C and 5C). PKC-dependent phosphorylation could mediate the exchange of ezrin for moesin once the cell is activated (of particular importance if their roles do not overlap), induce a conformational rearrangement in the CaM·L-selectin·ERM heterotrimeric complex triggering CaM dissociation, or affect the binding of additional partners to the cytoplasmic domain of L-selectin. Whether or not CaM

must dissociate for phosphorylation to occur remains to be determined.

A second, weaker binding site on CaM was observed for L-selectin (Figs. 1 and 6). This site maps to the "top" of the CaM molecule and could play a role in the clustering of L-selectin observed during leukocyte rolling *in vivo* or following triggering by antibodies or glycomimetics *in vitro* (66). By linking the cytoplasmic tails of two L-selectin receptors in *cis*, CaM could help to create a signaling platform that leads from the phosphorylation of L-selectin amino acid residue Tyr^{372} by the Src-tyrosine kinase p56^{lck} to the activation of Ras signaling pathways and the production of O_2^- (30, 67). This clustering pathway occurs prior to L-selectin ectodomain shedding in response to cell activation (6) and is thought to promote outside-in signals that lead to integrin activation and chemokine receptor activation and eventually leukocyte arrest.

L-selectin's rapid ectodomain shedding in response to cell activation is an anti-adhesive process that has an immediate influence on the accumulation of leukocytes along the vasculature wall and is required for neutrophil transendothelial migration into inflamed tissue (68, 69). Furthermore, shedding prevents antigen-activated T-cells from re-entering peripheral lymph nodes (70), and the released domains hinder leukocyte recruitment by reducing ligand availability, thus diminishing inflammation (71). Underscoring the physiological consequences of shedding, there are numerous clinical settings in which this phenomenon may either serve as a protective feedback mechanism or exacerbate existing pathologies (72, 73). By better understanding the cellular and molecular mechanisms of this process, including the role of CaM in activation-induced cleavage, it may be possible to produce therapies that manipulate shedding of the extracellular domains of L-selectin. The NMR solution structure presented here provides the first molecular details for a mechanism through which CaM negatively regulates the shedding of the extracellular domains of L-selectin. Furthermore, it highlights the role of calcium-signaling pathways in the observed shedding response to GPCR- or immunoreceptor-based cell activation.

REFERENCES

1. Ley, K., and Kansas, G. S. (2004) Selectins in T-cell recruitment to nonlymphoid tissues and sites of inflammation. *Nat. Rev. Immunol.* **4,** 325–335
2. Niggli, V. (2003) Signaling to migration in neutrophils. Importance of localized pathways. *Int. J. Biochem. Cell Biol.* **35,** 1619–1638
3. Ley, K., Laudanna, C., Cybulsky, M. I., and Nourshargh, S. (2007) Getting to the site of inflammation. The leukocyte adhesion cascade updated. *Nat. Rev. Immunol.* **7,** 678–689
4. Ivetic, A., and Ridley, A. J. (2004) The telling tail of L-selectin. *Biochem. Soc. Trans.* **32,** 1118–1121
5. Wedepohl, S., Beceren-Braun, F., Riese, S., Buscher, K., Enders, S., Bernhard, G., Kilian, K., Blanchard, V., Dernedde, J., and Tauber, R. (2012) L-selectin. A dynamic regulator of leukocyte migration. *Eur. J. Cell Biol.* **91,** 257–264
6. Xu, T., Chen, L., Shang, X., Cui, L., Luo, J., Chen, C., Ba, X., and Zeng, X. (2008) Critical role of Lck in L-selectin signaling induced by sulfatide

engagement. *J. Leukoc. Biol.* **84,** 1192–1201

7. Smalley, D. M., and Ley, K. (2005) L-selectin. Mechanisms and physiological significance of ectodomain cleavage. *J. Cell Mol. Med.* **9,** 255–266

8. Peschon, J. J., Slack, J. L., Reddy, P., Stocking, K. L., Sunnarborg, S. W., Lee, D. C., Russell, W. E., Castner, B. J., Johnson, R. S., Fitzner, J. N., Boyce, R. W., Nelson, N., Kozlosky, C. J., Wolfson, M. F., Rauch, C. T., Cerretti, D. P., Paxton, R. J., March, C. J., and Black, R. A. (1998) An essential role for ectodomain shedding in mammalian development. *Science* **282,** 1281–1284

9. Chin, D., and Means, A. R. (2000) Calmodulin. A prototypical calcium sensor. *Trends Cell Biol.* **10,** 322–328

10. Yamniuk, A. P., and Vogel, H. J. (2004) Calmodulin's flexibility allows for promiscuity in its interactions with target proteins and peptides. *Mol. Biotechnol.* **27,** 33–57

11. Kahn, J., Walcheck, B., Migaki, G. I., Jutila, M. A., and Kishimoto, T. K. (1998) Calmodulin regulates L-selectin adhesion molecule expression and function through a protease-dependent mechanism. *Cell* **92,** 809–818

12. Matala, E., Alexander, S. R., Kishimoto, T. K., and Walcheck, B. (2001) The cytoplasmic domain of L-selectin participates in regulating L-selectin endoproteolysis. *J. Immunol.* **167,** 1617–1623

13. Chen, A., Engel, P., and Tedder, T. F. (1995) Structural requirements regulate endoproteolytic release of the L-selectin (CD62L) adhesion receptor from the cell surface of leukocytes. *J. Exp. Med.* **182,** 519–530

14. Migaki, G. I., Kahn, J., and Kishimoto, T. K. (1995) Mutational analysis of the membrane-proximal cleavage site of L-selectin. Relaxed sequence specificity surrounding the cleavage site. *J. Exp. Med.* **182,** 549–557

15. Gifford, J. L., Ishida, H., and Vogel, H. J. (2011) Fast methionine-based solution structure determination of calcium-calmodulin complexes. *J. Biomol. NMR* **50,** 71–81

16. Bax, A., Delaglio, F., Grzesiek, S., and Vuister, G. W. (1994) Resonance assignment of methionine methyl groups and $\chi 3$ angular information from long-range proton-carbon and carbon-carbon J correlation in a calmodulin-peptide complex. *J. Biomol. NMR* **4,** 787–797

17. Ottiger, M., Delaglio, F., and Bax, A. (1998) Measurement of J and dipolar couplings from simplified two-dimensional NMR spectra. *J. Magn. Reson.* **131,** 373–378

18. Mal, T. K., Skrynnikov, N. R., Yap, K. L., Kay, L. E., and Ikura, M. (2002) Detecting protein kinase recognition modes of calmodulin by residual dipolar couplings in solution NMR. *Biochemistry* **41,** 12899–12906

19. Delaglio, F., Grzesiek, S., Vuister, G. W., Zhu, G., Pfeifer, J., and Bax, A. (1995) NMRPipe. A multidimensional spectral processing system based on UNIX pipes. *J. Biomol. NMR* **6,** 277–293

20. Johnson, B. A., and Blevins, R. A. (1994) NMR View. A computer program for the visualization and analysis of NMR data. *J. Biomol. NMR* **4,** 603–614

21. Grzesiek, S., Bax, A., Clore, G. M., Gronenborn, A. M., Hu, J. S., Kaufman, J., Palmer, I., Stahl, S. J., and Wingfield, P. T. (1996) The solution structure of HIV-1 Nef reveals an unexpected fold and permits delineation of the binding surface for the SH3 domain of Hck tyrosine protein kinase. *Nat. Struct. Biol.* **3,** 340–345

22. Zweckstetter, M., and Bax, A. (2000) Prediction of sterically induced alignment in a dilute liquid crystalline phase. Aid to protein structure determination by NMR. *J. Am. Chem. Soc.* **122,** 3791–3792

23. Ishida, H., and Vogel, H. J. (2006) Protein-peptide interaction studies demonstrate the versatility of calmodulin target protein binding. *Protein Pept. Lett.* **13,** 455–465

24. Guntert, P. (2003) Automated NMR protein structure calculation. *Prog. Nucl. Magn. Reson. Spectrosc.* **43,** 105–125

25. Cornilescu, G., Delaglio, F., and Bax, A. (1999) Protein backbone angle restraints from searching a database for chemical shift and sequence homology. *J. Biomol. NMR* **13,** 289–302

26. Chou, J. J., Li, S., and Bax, A. (2000) Study of conformational rearrangement and refinement of structural homology models by the use of heteronuclear dipolar couplings. *J. Biomol. NMR* **18,** 217–227

27. Huang, H., Ishida, H., Yamniuk, A. P., and Vogel, H. J. (2011) Solution structures of Ca^{2+}-CIB1 and Mg^{2+}-CIB1 and their interactions with the platelet integrin αIIb cytoplasmic domain. *J. Biol. Chem.* **286,** 17181–17192

28. Morris, A. L., MacArthur, M. W., Hutchinson, E. G., and Thornton, J. M. (1992) Stereochemical quality of protein structure coordinates. *Proteins* **12,** 345–364

29. Koradi, R., Billeter, M., and Wüthrich, K. (1996) MOLMOL. A program for display and analysis of macromolecular structures. *J. Mol. Graph.* **14,** 51–55, 29–32

30. Killock, D. J., Parsons, M., Zarrouk, M., Ameer-Beg, S. M., Ridley, A. J., Haskard, D. O., Zvelebil, M., and Ivetic, A. (2009) *In vitro* and *in vivo* characterization of molecular interactions between calmodulin, ezrin/radixin/moesin, and L-selectin. *J. Biol. Chem.* **284,** 8833–8845

31. Ramachandran, S., Kota, P., Ding, F., and Dokholyan, N. V. (2011) Automated minimization of steric clashes in protein structures. *Proteins* **79,** 261–270

32. Yamniuk, A. P., Burling, H., and Vogel, H. J. (2009) Thermodynamic characterization of the interactions between the immunoregulatory proteins osteopontin and lactoferrin. *Mol. Immunol.* **46,** 2395–2402

33. Rainaldi, M., Yamniuk, A. P., Murase, T., and Vogel, H. J. (2007) Calcium-dependent and -independent binding of soybean calmodulin isoforms to the calmodulin binding domain of tobacco MAPK phosphatase-1. *J. Biol. Chem.* **282,** 6031–6042

34. Ikura, M., Kay, L. E., Krinks, M., and Bax, A. (1991) Triple-resonance multidimensional NMR study of calmodulin complexed with the binding domain of skeletal muscle myosin light-chain kinase. Indication of a conformational change in the central helix. *Biochemistry* **30,** 5498–5504

35. Contessa, G. M., Orsale, M., Melino, S., Torre, V., Paci, M., Desideri, A., and Cicero, D. O. (2005) Structure of calmodulin complexed with an olfactory CNG channel fragment and role of the central linker. Residual dipolar couplings to evaluate calmodulin binding modes outside the kinase family. *J. Biomol. NMR* **31,** 185–199

36. Lipsitz, R. S., and Tjandra, N. (2004) Residual dipolar couplings in NMR structure analysis. *Annu. Rev. Biophys. Biomol. Struct.* **33,** 387–413

37. Fallon, J. L., Halling, D. B., Hamilton, S. L., and Quiocho, F. A. (2005). Structure of calmodulin bound to the hydrophobic IQ domain of the cardiac Ca(v)1.2 calcium channel. *Structure* **13,** 1881–1886

38. Ruschak, A. M., and Kay, L. E. (2010) Methyl groups as probes of supramolecular structure, dynamics, and function. *J. Biomol. NMR* **46,** 75–87

39. Yamniuk, A. P., Ishida, H., Lippert, D., and Vogel, H. J. (2009) Thermodynamic effects of noncoded and coded methionine substitutions in calmodulin. *Biophys. J.* **96,** 1495–1507

40. Ishida, H., Rainaldi, M., and Vogel, H. J. (2009) Structural studies of soybean calmodulin isoform 4 bound to the calmodulin-binding domain of tobacco mitogen-activated protein kinase phosphatase-1 provide insights into a sequential target binding mode. *J. Biol. Chem.* **284,** 28292–28305

41. Yuan, T., Weljie, A. M., and Vogel, H. J. (1998) Tryptophan fluorescence quenching by methionine and selenomethionine residues of calmodulin. Orientation of peptide and protein binding. *Biochemistry* **37,** 3187–3195

42. Ivetic, A., Florey, O., Deka, J., Haskard, D. O., Ager, A., and Ridley, A. J. (2004) Mutagenesis of the ezrin-radixin-moesin binding domain of L-selectin tail affects shedding, microvillar positioning, and leukocyte tethering. *J. Biol. Chem.* **279,** 33263–33272

43. Killock, D. J., and Ivetić, A. (2010) The cytoplasmic domains of TNFalpha-converting enzyme (TACE/ADAM17) and L-selectin are regulated differently by p38 MAPK and PKC to promote ectodomain shedding. *Biochem. J.* **428,** 293–304

44. Ivetic, A., Deka, J., Ridley, A., and Ager, A. (2002) The cytoplasmic tail of L-selectin interacts with members of the ezrin-radixin-moesin (ERM) family of proteins. Cell activation-dependent binding of Moesin but not Ezrin. *J. Biol. Chem.* **277,** 2321–2329

45. Berridge, M. J. (2006) Calcium microdomains. Organization and function. *Cell Calcium* **40,** 405–412

46. Laudanna, C., Constantin, G., Baron, P., Scarpini, E., Scarlato, G., Cabrini, G., Dechecchi, C., Rossi, F., Cassatella, M. A., and Berton, G. (1994) Sulfatides trigger increase of cytosolic free calcium and enhanced expression of tumor necrosis factor-α and interleukin-8 mRNA in human neutrophils. Evidence for a role of L-selectin as a signaling molecule. *J. Biol. Chem.* **269,** 4021–4026

47. Krummel, M. F., and Cahalan, M. D. (2010) The immunological synapse. A dynamic platform for local signaling. *J. Clin. Immunol.* **30,** 364–372

48. Vig, M., and Kinet, J. P. (2009) Calcium signaling in immune cells. *Nat.*

Immunol. **10,** 21–27

49. Gifford, J. L., Walsh, M. P., and Vogel, H. J. (2007) Structures and metal ion-binding properties of the Ca^{2+}-binding helix-loop-helix EF-hand motifs. *Biochem. J.* **405,** 199–221

50. Furukawa, Y., Umemoto, E., Jang, M. H., Tohya, K., Miyasaka, M., and Hirata, T. (2008) Identification of novel isoforms of mouse L-selectin with different carboxyl-terminal tails. *J. Biol. Chem.* **283,** 12112–12119

51. Zhao, L., Shey, M., Farnsworth, M., and Dailey, M. O. (2001) Regulation of membrane metalloproteolytic cleavage of L-selectin (CD62l) by the epidermal growth factor domain. *J. Biol. Chem.* **276,** 30631–30640

52. Deng, W., Srinivasan, S., Zheng, X., Putkey, J. A., and Li, R. (2011) Interaction of calmodulin with L-selectin at the membrane interface. Implication in the regulation of L-selectin shedding. *J. Mol. Biol.* **411,** 220–233

53. Barry, W. T., Boudignon-Proudhon, C., Shock, D. D., McFadden, A., Weiss, J. M., Sondek, J., and Parise, L. V. (2002) Molecular basis of CIB binding to the integrin αIIb cytoplasmic domain. *J. Biol. Chem.* **277,** 28877–28883

54. Denofrio, J. C., Yuan, W., Temple, B. R., Gentry, H. R., and Parise, L. V. (2008) Characterization of calcium- and integrin-binding protein 1 (CIB1) knockout platelets. Potential compensation by CIB family members. *Thromb. Haemost.* **100,** 847–856

55. Huang, H., and Vogel, H. J. (2012) Structural basis for the activation of platelet integrin αIIbβ3 by calcium- and integrin-binding protein 1. *J. Am. Chem. Soc.* **134,** 3864–3872

56. Naik, U. P., and Naik, M. U. (2003) Association of CIB with GPIIb/IIIa during outside-in signaling is required for platelet spreading on fibrinogen. *Blood* **102,** 1355–1362

57. Yamniuk, A. P., Ishida, H., and Vogel, H. J. (2006) The interaction between calcium- and integrin-binding protein 1 and the αIIb integrin cytoplasmic domain involves a novel C-terminal displacement mechanism. *J. Biol. Chem.* **281,** 26455–26464

58. Yuan, W., Leisner, T. M., McFadden, A. W., Wang, Z., Larson, M. K., Clark, S., Boudignon-Proudhon, C., Lam, S. C., and Parise, L. V. (2006) CIB1 is an endogenous inhibitor of agonist-induced integrin αIIbβ3 activation. *J. Cell Biol.* **172,** 169–175

59. Lai, Z. W., Lew, R. A., Yarski, M. A., Mu, F. T., Andrews, R. K., and Smith, A. I. (2009) The identification of a calmodulin-binding domain within the cytoplasmic tail of angiotensin-converting enzyme-2. *Endocrinology* **150,** 2376–2381

60. Locke, D., Liu, C., Peng, X., Chen, H., and Kahn, M. L. (2003) FcRγ-independent signaling by the platelet collagen receptor glycoprotein VI. *J. Biol. Chem.* **278,** 15441–15448

61. Wong, M. X., Harbour, S. N., Wee, J. L., Lau, L. M., Andrews, R. K., and Jackson, D. E. (2004) Proteolytic cleavage of platelet endothelial cell adhesion molecule-1 (PECAM-1/CD31) is regulated by a calmodulin-binding motif. *FEBS Lett.* **568,** 70–78

62. Haribabu, B., Steeber, D. A., Ali, H., Richardson, R. M., Snyderman, R., and Tedder, T. F. (1997) Chemoattractant receptor-induced phosphorylation of L-selectin. *J. Biol. Chem.* **272,** 13961–13965

63. Kilian, K., Dernedde, J., Mueller, E. C., Bahr, I., and Tauber, R. (2004) The interaction of protein kinase C isozymes α, ι, and θ with the cytoplasmic domain of L-selectin is modulated by phosphorylation of the receptor. *J. Biol. Chem.* **279,** 34472–34480

64. Mattila, P. E., Green, C. E., Schaff, U., Simon, S. I., and Walcheck, B. (2005) Cytoskeletal interactions regulate inducible L-selectin clustering. *Am. J. Physiol. Cell Physiol.* **289,** C323–C332

65. Schaff, U., Mattila, P. E., Simon, S. I., and Walcheck, B. (2008) Neutrophil adhesion to E-selectin under shear promotes the redistribution and co-clustering of ADAM17 and its proteolytic substrate L-selectin. *J. Leukoc. Biol.* **83,** 99–105

66. Zarbock, A., and Ley, K. (2008) Mechanisms and consequences of neutrophil interaction with the endothelium. *Am. J. Pathol.* **172,** 1–7

67. Brenner, B., Gulbins, E., Schlottmann, K., Koppenhoefer, U., Busch, G. L., Walzog, B., Steinhausen, M., Coggeshall, K. M., Linderkamp, O., and Lang, F. (1996) L-selectin activates the Ras pathway via the tyrosine kinase p56^{lck}. *Proc. Natl. Acad. Sci. U.S.A.* **93,** 15376–15381

68. Li, Y., Brazzell, J., Herrera, A., and Walcheck, B. (2006) ADAM17 deficiency by mature neutrophils has differential effects on L-selectin shedding. *Blood* **108,** 2275–2279

69. Venturi, G. M., Tu, L., Kadono, T., Khan, A. I., Fujimoto, Y., Oshel, P., Bock, C. B., Miller, A. S., Albrecht, R. M., Kubes, P., Steeber, D. A., and Tedder, T. F. (2003) Leukocyte migration is regulated by L-selectin endoproteolytic release. *Immunity* **19,** 713–724

70. Galkina, E., Tanousis, K., Preece, G., Tolaini, M., Kioussis, D., Florey, O., Haskard, D. O., Tedder, T. F., and Ager, A. (2003) L-selectin shedding does not regulate constitutive T cell trafficking but controls the migration pathways of antigen-activated T lymphocytes. *J. Exp. Med.* **198,** 1323–1335

71. Tu, L., Poe, J. C., Kadono, T., Venturi, G. M., Bullard, D. C., Tedder, T. F., and Steeber, D. A. (2002) A functional role for circulating mouse L-selectin in regulating leukocyte/endothelial cell interactions *in vivo*. *J. Immunol.* **169,** 2034–2043

72. Strausbaugh, H. J., Green, P. G., Lo, E., Tangemann, K., Reichling, D. B., Rosen, S. D., and Levine, J. D. (1999) Painful stimulation suppresses joint inflammation by inducing shedding of L-selectin from neutrophils. *Nat. Med.* **5,** 1057–1061

73. Thiel, M., Zourelidis, C., Chambers, J. D., von Andrian, U. H., Arfors, K. E., Messmer, K., and Peter, K. (1997) Expression of β2-integrins and L-selectin on polymorphonuclear leukocytes in septic patients. *Eur. Surg Res.* **29,** 160–175

74. Larkin, M. A., Blackshields, G., Brown, N. P., Chenna, R., McGettigan, P. A., McWilliam, H., Valentin, F., Wallace, I. M., Wilm, A., Lopez, R., Thompson, J. D., Gibson, T. J., and Higgins, D. G. (2007) ClustalW and ClustalX version 2.0. *Bioinformatics* **23,** 2947–2948

75. Yap, K. L., Kim, J., Truong, K., Sherman, M., Yuan, T., and Ikura, M. (2000) Calmodulin target database. *J. Struct. Funct. Genomics* **1,** 8–14

76. Hirokawa, T., Boon-Chieng, S., and Mitaku, S. (1998) SOSUI. Classification and secondary structure prediction system for membrane proteins. *Bioinformatics* **14,** 378–379